Journal of Catalysis 305 (2013) 118–129

Contents lists available at SciVerse ScienceDirect

Journal of Catalysis

journal homepage: www.elsevier.com/locate/jcat

Insight in the activity and diastereoselectivity of various Lewis acid catalysts for the citronellal cyclization

Matthias Vandichel [a,b], Frederik Vermoortele [c], Stijn Cottenie [a,b], Dirk E. De Vos [c,*], Michel Waroquier [a,b], Veronique Van Speybroeck [a,b,*]

[a] Center for Molecular Modeling (CMM), Ghent University, Technologiepark 903, 9052 Zwijnaarde, Belgium
[b] QCMM-Alliance, Ghent-Brussels, Belgium
[c] Centre for Surface Chemistry and Catalysis, Katholieke Universiteit Leuven, Kasteelpark Arenberg 23, 3001 Leuven, Belgium

ARTICLE INFO

Article history:
Received 1 February 2013
Revised 30 March 2013
Accepted 22 April 2013

Keywords:
Lewis acids
Selectivity
Activity
Heterogeneous catalysis
Chemical kinetics
Citronellal cyclization
Cu-BTC
ATPH
$ZnBr_2$
Diastereoselective catalysis

ABSTRACT

Industrial (−)-menthol production generally relies on the hydrogenation of (−)-isopulegol, which is in turn produced with high selectivity by cyclization of (+)-citronellal. This paper uses a combined theoretical and experimental approach to study the activity and selectivity of three Lewis acid catalysts for this reaction, namely $ZnBr_2$, aluminum tris(2,6-diphenylphenoxide) (ATPH), and the heterogeneous metal–organic framework Cu_3BTC_2 (BTC = benzene-1,3,5-tricarboxylate). ATPH is a strong Lewis acid homogeneous catalyst with bulky ligands which provides very high selectivities for the desired stereoisomer (>99%). The performance of the catalysts was evaluated as a function of temperature, which revealed that a higher catalyst activity allows working at lower temperatures and improves the selectivity for isopulegol. The selectivity distribution is kinetically driven for $ZnBr_2$ and ATPH. The theoretical selectivity distributions rely on the determination of an extensive set of diastereomeric transition states, for which the differences in free energy have been calculated using a complementary set of ab initio techniques. Given the sensitivity of the selectivity to small Gibbs free-energy differences, the agreement between experimental and theoretical selectivities is satisfactory. On basis of the obtained insights, rational design of new catalysts may be obtained. As proof of concept, the hypothetical $Cu_3(BTC\text{-}(NO_2)_3)_2$ Lewis catalyst – in which each phenyl hydrogen of the BTC ligand is replaced by a nitro group – is predicted to be very selective.

1. Introduction

The cyclization of citronellal to isopulegol is an important step in the production of menthol, which is worldwide one of the most important flavor chemicals. The overall demand for menthol is partly met by isolation from natural sources, but mainly by chemical synthesis. In 2010, 19,300 tons of (−)-menthol were produced naturally or synthetically, making this product one of the largest volume chiral chemicals in the world [1]. Of the eight stereoisomers of menthol, only (−)-menthol possesses the characteristic peppermint odor and physiological cooling effect. Various synthesis procedures have been designed for the preparation of (−)-menthol [2]. Two processes, established by Takasago and BASF, have the cyclization of (+)-citronellal as an intermediate step. This reaction is usually conducted over a Lewis acid catalyst and can lead to four diastereoisomers, namely isopulegol, iso-isopulegol, neo-isopulegol, and neoiso-isopulegol (Scheme 1).

With Lewis acids, high selectivities may be obtained especially when using metal halogenides (selectivity of about 86% at 110 °C and 93% at 25 °C with $ZnBr_2$ as catalyst [3]). With Brønsted acids, the selectivity is significantly lower but still (−)-isopulegol is the most abundant product. The reaction is also sensitive to side reactions such as subsequent, cracking, or dehydration [4–6].

The more recent BASF process uses tris(2,6-diarylaryloxy)aluminum catalysts, especially the tris(2,6-diphenylphenoxy)aluminum complex [7–10] (ATPH) which has an (−)-isopulegol selectivity of more than 99% [7]. Very recently, Itoh and Hori found that aryl binol ligands in combination with Al also form a selective catalyst for the citronellal cyclization [11].

Apart from these homogeneous catalysts, several solid acid materials have been explored [12,13]. Promising concepts have been explored using zeolites containing isolated and well-defined Lewis acid centers, such as Sn and Zr atoms [14,15]. Recently, the spectrum of nanoporous materials has been further expanded to metal organic frameworks (MOFs). Those materials, consisting of both inorganic and organic moieties, have been applied in many different areas, ranging from gas storage [16–22], gas separation

* Corresponding authors at: Centre for Surface Chemistry and Catalysis, Katholieke Universiteit Leuven, Kasteelpark Arenberg 23, 3001 Leuven, Belgium (D.E.De Vos), Center for Molecular Modeling (CMM), Ghent University, Technologiepark 903, 9052 Zwijnaarde, Belgium (V. Van Speybroeck).
E-mail addresses: dirk.devos@biw.kuleuven.be (D.E. De Vos), veronique.vanspeybroeck@ugent.be (V. Van Speybroeck).

0021-9517/$ - see front matter © 2013 Elsevier Inc. All rights reserved.
http://dx.doi.org/10.1016/j.jcat.2013.04.017

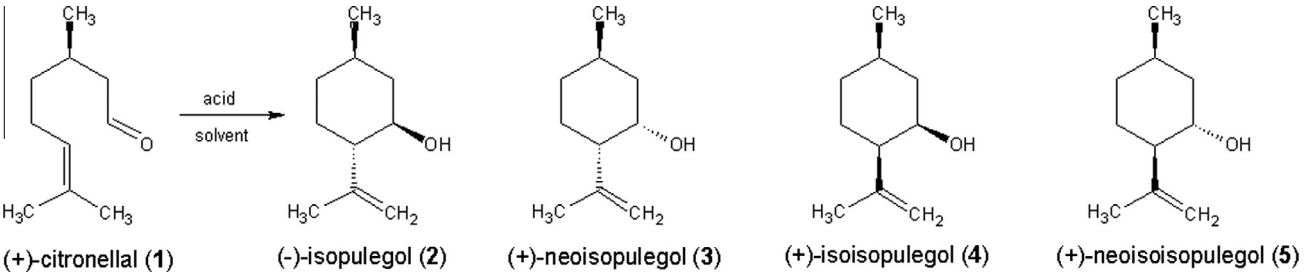

Scheme 1. The acid-catalyzed cyclization of (+)-citronellal (**1**) yields four different isopulegol isomers: (−)-isopulegol (**2**), (+)-neoisopulegol (**3**), (+)-isoisopulegol (**4**), and (+)-neoisoisopulegol (**5**).

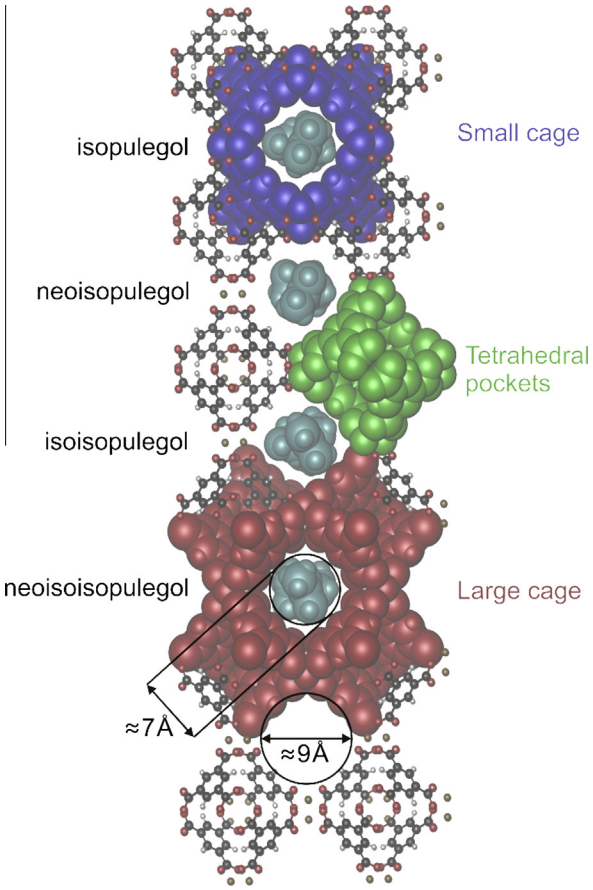

Fig. 1. Cu_3BTC_2; the cut through the crystals shows the two types of cages, with various isopulegol isomers located in the pore window.

[23–26], luminescent properties [27–29], magnetic properties [22,30], etc. Also in the field of heterogeneous catalysis [16,22,31–34], major progress has been made in initial experimental studies investigating the catalytic properties of MOFs. Some of the present authors investigated the cyclization of citronellal on Cu_3BTC_2 [35] [BTC = benzene-1,3,5-tricarboxylate] and found selectivities for the desired product isopulegol of 65% up to 69% dependent on the solvent used. Cu_3BTC_2 (hereafter abbreviated with Cu-BTC) has taken a prominent role within the field of MOF research for various applications, because of open Cu^{2+} coordination sites in combination with a structure exhibiting both large and small cages (Fig. 1) [36,37]. Based on the pore size, this structure seems to allow diffusion of reactants and products, such as citronellal and isopulegol isomers in and out of the cages. Previous studies on the catalytic activity of Cu-BTC in various reactions have shown the hard Lewis acid behavior of the material [35,38–41] [42].

The principal goal of this paper is to study the industrially important citronellal cyclization [1,43] on various catalysts, i.e., $ZnBr_2$, ATPH and Cu-BTC, to achieve insight into the factors controlling the activity and selectivity for this diastereoselective reaction. Such insight is important to rationally design new heterogeneous catalysts for this important industrial process. A combined theoretical and experimental approach has been followed. Experimentally, the reaction rates and selectivities for the dominant isomer using different catalysts were determined in various temperature intervals. To obtain insight into the molecular factors controlling both activity and selectivity, a thorough molecular modeling approach was conducted. The full reactive profile was calculated by means of first-principles calculations, including the adsorption and desorption steps. A theoretical selectivity model is set up that relies on the construction of a set of transition states. The combined approach followed here is a step in the rational design of diastereoselective catalysts for the citronellal cyclization. As a proof of concept, the hypothetical $Cu_3(BTC\text{-}(NO_2)_3)_2$ MOF structure is introduced, inspired by previous results on ligand effects on MOF catalysis [44].

2. Computational and experimental methods

2.1. Computational methods

2.1.1. Cluster calculations

All cluster calculations were performed with the Gaussian09 package [45]. We used the B3LYP/6-311++g(3df,2p) level of theory for the geometry optimization of $ZnBr_2$. For the two other catalysts (Cu-BTC and ATPH), modeled by more extended clusters, we make use of the well-established ONIOM-scheme. This multi-layer method allows for a fast optimization of the geometries. The smaller part of the cluster is described at a higher level of theory (we have chosen for B3LYP/6-31+G(d)) and the rest at a lower level of theory (B3LYP/3-21g). For the copper metal in Cu-BTC, we used the LANL2DZ basis set and pseudopotential [46]. This combined basis will be abbreviated as BS1 for further use. Once geometry optimizations have been achieved, we systematically perform energy refinements by redoing the calculations with a triple-zeta Pople basis set with diffuse and polarization functions (basis set B3LYP/6-311+g(d,p)) on each of the three catalysts. To account for dispersion effects, Grimme corrections of the type D3 [47] were added afterward to refine the energies, using the dftd3 program available from the authors' web site. Specific for the Cu-BTC cluster is the spin multiplicity which uniformly is taken as 3 in all structures (transition states, adsorbed complexes, etc.). The above outlined level of theory has been consistently applied for the computation of the catalyst activity for the citronellal cyclization.

A reliable theoretical prediction of the diastereoselectivity of the three catalysts for the citronellal cyclization requires very accurate energy differences between the various transition states occurring in the cyclization process and leading to the four isopulegol isomers (Section 3.3). In view of the structure of ATPH, we opted to apply an even more advanced functional (M06-2X hybrid

functional [48,49]), which is a good choice to accurately quantify the adsorbate–ligand interactions and ligand–ligand interactions because it is used especially for medium range non-covalent interactions. In this functional, double Hartree–Fock exchange is included to improve the description of non-covalent interactions [50,51]. Concluding, for ATPH, the selectivities were computed from transition state structures constructed with the ONIOM(M06-2X/6-31+g(d):M06-2X/3-21g) level of theory. For the other catalysts, there was no need to introduce new functionals for the selectivity calculations and the same functional and basis set B3LYP/6-311+g(d,p), as employed for the activity predictions, have been used.

The construction of the extended cluster representing Cu-BTC has been done as usual (a similar procedure was also applied previously for the description of active sites within the Metal Organic Framework MIL-47 [52]): a sufficiently large moiety (Cu_2BTC_4) was cut from the optimized Cu-BTC unit cell after periodic extension in Zeobuilder [53] and saturated by hydrogen atoms. The extended cluster is displayed in Fig. 2. The two adopted ONIOM layers are also shown: the active site is visualized in ball and stick, while the low level region is indicated in sticks. Analogously, the $Cu_2(BTC\text{-}(NO_2)_3)_4$ cluster (hereafter abbreviated with Cu-BTC-NO_2) was constructed arbitrarily by substituting all hydrogen atoms on the phenyl groups of the extended Cu-BTC cluster by NO_2-groups.

2.1.2. Periodic calculations

In addition to extended cluster calculations, also periodic calculations were performed on the metal organic framework Cu-BTC. They were executed with the Vienna Ab Initio Simulation Package (VASP) [54–57].

The transition states from the extended cluster calculations were taken as starting geometries to find the transition states in the periodic model. An optimized Cu-BTC unit-cell was obtained from Nachtigall et al. [58] and was re-optimized with periodic DFT-PBE-D2 calculations. For these simulations, the Brillouin zone was restricted to the Γ-point. We employed the PBE exchange correlation functional [59,60] and the projector augmented wave approximation (PAW) [61] together with a plane wave basis set (kinetic energy cutoff of 600 eV). The RMM-DIIS algorithm was chosen as optimizer to converge the atomic forces below 0.01 eV/Å. Furthermore, van der Waals corrections [62] for the PBE functional were used throughout the optimization, as implemented in the VASP 5.2.11 code. The convergence criterion for the electronic self-consistent field (SCF) problem is set to 10^{-8} eV. Displacements in *a*, *b*, and *c*-axis of ±0.015 Å are used in a subsequent partial Hessian calculation, where only the atoms of the $Cu_2(COO)_4$ paddlewheel and the reacting citronellal are taken into account. De Moor et al. [63] have shown that this type of procedure is sufficient to obtain a well-conditioned partial Hessian, which has only positive eigenmodes in case of a minimum and only one imaginary eigenmode in case of a transition state.

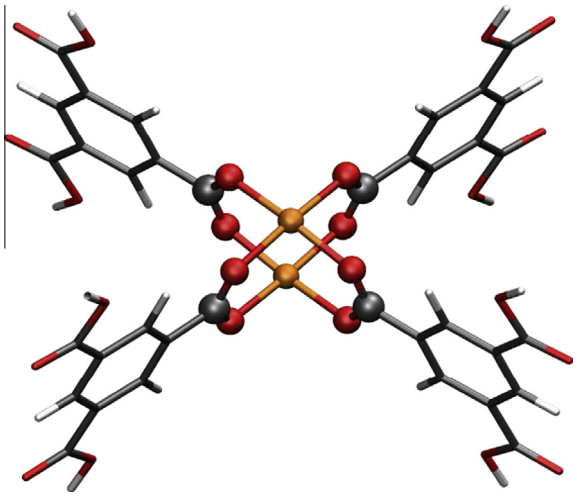

Fig. 2. The extended Cu_2BTC_4 cluster and the applied ONIOM-scheme. The high level (B3LYP/BS1) visualized in ball and stick; low level (B3LYP/3-21g) in sticks; outer carboxylic oxygen atoms were fixed upon optimization.

2.1.3. Construction of the transition states on the catalyst

A normal mode analysis was carried out to verify the nature of the transitions states and local minima. The PHVA method [45,64,65] was used for cluster and periodic models as implemented in the in-house developed post-processing toolkit TAMkin [66]. TAMkin has already proved its efficiency in the computation of reaction kinetics [44,67–69]. This program is used to investigate the kinetics and the activation barriers of the citronellal cyclization.

There exist many transition states leading to the different isopulegol diastereomers. They largely depend on the position of the citronellal in the adsorbed complex with the catalyst. A thorough exploration of the free-energy surface has been performed to ensure that all important transition states are taken into account, which is important for the selectivity determination. In Section 3.1, such a survey is outlined on the citronellal cyclization taking place on a $Cu_2(COO)_4$ paddlewheel. The most stable transition states exhibit a chair conformation of the adsorbate during the C—C coupling. The same procedure has been applied to the other catalysts and an overview of most of the lowest activated transition states is displayed in the Supplementary Material (SM). Not all different adsorption positions of citronellal on the catalyst lead to different transition state structures. Sometimes, they reproduce the same transition state (e.g., transition states toward neo-isopulegol **3** and neoiso-isopulegol **4** on $ZnBr_2$, we refer to Table S5 and Fig. S3). In this case, only a single adsorption geometry was considered in the selectivity analysis.

2.2. Theoretical methods to determine the selectivity

The computational prediction of diastereoselectivities of metal-catalyzed reactions is challenging, as it requires the calculation of small free-energy differences between diastereomeric transition states [64]. Therefore, high but feasible levels of theory are needed for the electronic energy calculations as outlined in the computational section (Section 2.1). A full conformational search of the diastereomeric transition states is required. A complete sampling of the free-energy surface in the vicinity of possible transition states can in principle be done using Monte Carlo or molecular dynamics methods. On the other hand, it is also essential to take the full catalytic structure into account to model appropriately the molecular environment and therefore such methods are computationally not feasible with the current methods from first-principles. One could opt for reliable molecular mechanics methods but unfortunately the parameters for transition metals are not readily available [65]. In view of previous considerations, we performed static calculations on the full catalytic system and constructed a set of low activated transition states in a very systematic way for each diastereomer and for each catalyst. Their differences in free-energy barrier are used as input for the further selectivity predictions. More detail on how we constructed this set for each catalyst is given in Section 2.1.3. Following this protocol, the selectivities toward the different isopulegol isomers can be calculated using the Curtin-Hammett principle. Hereby, we assume that all reactant conformations are in thermodynamic equilibrium and that only the free-energy differences between the transition states are important [66]. As such a measure for the relative selectivity

toward a specific isomer, i is given by the ratio defined by the rate of formation of isomer i relative to the total rate of formation:

$$S_{i,ini} = \frac{k_i^{app}}{\sum_j k_j^{app}} = \frac{k_i^{int}}{\sum_j k_j^{int}} \quad (1)$$

Herein, k_i^{app} is the apparent bimolecular rate coefficient ($m^3\ mol^{-1}$ - s^{-1}) for the cyclization reaction toward i-pulegol with $i \in \langle \text{iso, neoiso, isoiso, neoisoiso} \rangle$. The apparent kinetics differ from the intrinsic kinetics in that in the former the kinetic data are referred to the catalyst and the citronellal molecule in gas phase, while the intrinsic kinetic data are referred to the whole adsorbed complex. If we assume that each reaction leading to a specific isopulegol i starts from the same reactant complex, the relative selectivity may even be expressed in terms of the intrinsic and unimolecular rate coefficients k_i^{int} (s^{-1}). The equality in Eq. (1) can easily be proven by introducing Gibbs free energies for the transition states and by making use of a constant free energy of adsorption ΔG_{ads} for the fully adsorbed citronellal-catalyst complex. As the rate constant k_i is proportional to $\exp\left(-\frac{\Delta G_i^{\ddagger}}{RT}\right)$, the relative selectivity may also be written as:

$$S_{i,ini} = \frac{\exp\left(-\frac{\Delta G_i^{\ddagger}(app)}{RT}\right)}{\sum_j \exp\left(-\frac{\Delta G_j^{\ddagger}(app)}{RT}\right)} = \frac{\exp\left(-\frac{\Delta G_i^{\ddagger}(int)}{RT}\right)}{\sum_j \exp\left(-\frac{\Delta G_j^{\ddagger}(int)}{RT}\right)} \quad (2)$$

Eqs. (1) and (2) are valid in the initial stages of the reaction, as they take only the forward reaction rates into consideration. So in the assumption of Eq. (1), (2), the citronellal cyclization reactions are considered as irreversible.

An alternative method to calculate the selectivities is based on thermodynamic grounds, taking only the thermodynamic product equilibrium (TPE) into account. As such the selectivity toward isomer i of pulegol becomes:

$$S_{i,TPE} = \frac{c_{i,E}}{\sum_j c_{j,E}} = \frac{\exp\left(-\frac{\Delta G_i^{prod}}{RT}\right)}{\sum_j \exp\left(-\frac{\Delta G_j^{prod}}{RT}\right)} \quad (3)$$

with $c_{i,E}$ the equilibrium concentration of the i-pulegol and G_j^{prod} the free energy of isopulegol j in the product state. As the product concentration increases, the backward reaction becomes more and more important and the selectivity is expected to be more and more thermodynamically driven. It is not excluded that the experimental selectivity on each catalyst will take a value between the initial selectivity $S_{i,ini}$ and the product determined selectivity $S_{i,TPE}$.

2.3. Experimental catalyst preparation

ATPH was synthesized as reported in Ref. [67]: 240 mg 2,6-diphenylphenol was dissolved in 5 ml of (dry) toluene and flushed with argon at room temperature. Under Ar-atmosphere, 150 mg of a 25 wt% solution triethylaluminium in toluene was added and the mixture was stirred at room temperature for 30 min.

Cu-BTC was synthesized in the microwave oven using a procedure published by Seo et al. [68]. Two different solutions were made:

(1) 1.764 g $Cu(NO_3)_2$ trihydrate in 24 ml H_2O.
(2) 0.840 g BTC in 24 ml EtOH.

The two clear solutions were mixed together and placed in the microwave oven. The solution was heated to 140 °C in 10 min and kept at this temperature for 2 h. After synthesis, the materials were thoroughly washed with a 1:1 ethanol–water mixture and dried at 100 °C. The quality and crystallinity of Cu-BTC were verified by powder X-ray diffraction measurements (Fig. 3).

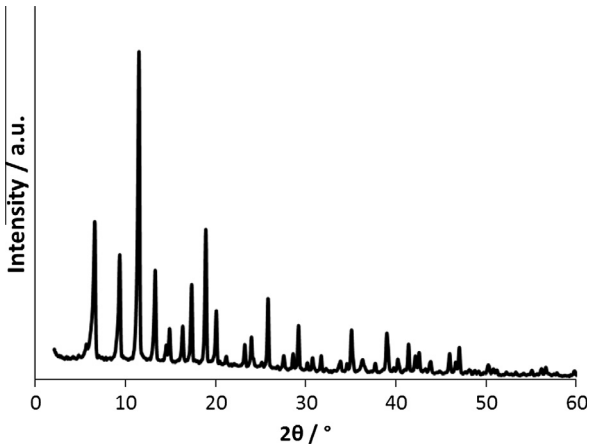

Fig. 3. Powder X-ray diffraction measurement on Cu-BTC.

Anhydrous $ZnBr_2$ (98%, Fluka) was used as received.

2.4. Experimental determination of the initial selectivity

Experimental initial selectivities were determined at low citronellal conversion (5–15%) on ATPH, $ZnBr_2$, and Cu-BTC. The reactions were carried out at different temperatures, and the experimental values were corrected for the thermal reaction using the following equations:

$$X = X_{cat} - X_0 \quad (4)$$

in which X_{cat} is the obtained conversion of citronellal after reaction over the catalyst while X_0 is the conversion obtained with a thermal reaction over the same time. The initial experimental selectivity $S_{i,ini,exp}$ was computed as follows:

$$S_{i,ini,exp} = \frac{S_{i,cat}X_{cat} - S_{i,0}X_0}{X_{cat} - X_0} \quad (5)$$

In Eq. (5), $S_{i,cat}$ is the selectivity toward isopulegol with the catalyst while $S_{i,0}$ represents the selectivity toward isopulegol ($i \in \langle \text{iso, neoiso, isosiso, neoisosio} \rangle$) in the thermal reaction.

Reactions using **$ZnBr_2$** and **Cu-BTC** as a catalyst were carried out without solvent. 1 g of citronellal was added to 0.1 g of catalyst in a glass vial. A Teflon coated stirring bar was added, and the glass vials were placed in copper block equipped with a thermocouple. For **ATPH**, 0.5 g citronellal was added dropwise to a stirred solution of 0.164 mmol ATPH in 2.5 ml toluene at 298 K. After a short reaction time (between 5 and 15 min), the reaction was stopped by adding 2 ml of a 4% NaOH solution. Before analysis, the reaction mixture was filtered through a 0.2-μm HPLC filter. 1 ml of toluene was added to 0.2 ml of the product and analyzed using gas chromatography.

3. Results and discussion

3.1. Mechanism of the citronellal cyclization on Lewis acid catalysts

It is commonly accepted that the cyclization of citronellal occurs through a concerted mechanism [44,69–71]. More details regarding the reaction mechanism of a standard carbonyl-ene reaction [72] are given in Section 1 of the Supplementary Material (SM). Citronellal cyclization has also been investigated on solid Lewis acid catalysts. In the work of Boronat et al. [12,13], tin atoms

were incorporated into the Beta zeolite framework (Sn-Beta) and of a more confined MFI zeolite. They found that the substrate was activated by coordination of the carbonyl group to the Lewis acid Sn center [12]. The diastereoselective cyclization of citronellal derivatives has also been investigated in a combined experimental–theoretical work by Kikukawa et al. [73] with Lewis acid sites generated in aluminum compounds, more specifically dialuminum-substituted silicotungstate. This compound showed a high catalytic activity for the cyclization and selectivity for the various isopolegol isomers including a very high diastereoselectivity toward **2**. A DFT calculation on citronellal cyclization in the gas phase revealed that the reaction proceeds through an asynchronous concerted mechanism [74]. Very recently, we demonstrated by means of a combined theoretical and experimental study that electronic linker modulations of the Zr-terephthalate MOF UiO-66 (UiO-66-X) remarkably increase the catalytic activity for the citronellal cyclization [44].

In this study, a thorough investigation is performed on the cyclization of citronellal on various catalysts to assess their relative selectivity toward (−)-isopulegol and their relative activity. The transition states toward the major isomer, (−)-isopulegol, for the reaction occurring in gas phase and on the Lewis acid catalysts $ZnBr_2$, Cu-BTC and ATPH are shown in Fig. 4. All localized transition state geometries confirm the concerted nature of the reaction, during which a nucleophilic attack occurs of the C=C double bond to the carbonyl group forming a new carbon–carbon bond with simultaneous transfer of a hydrogen of one of the methyl groups toward the carbonyl group, yielding a hydroxyl group. Furthermore, the concerted nature of the transition states was confirmed by Intrinsic Reaction Coordinate (IRC) calculations. In order to obtain reasonable reaction rates, the carbonyl group needs to be activated on a Lewis acid metal center. The various transition states depicted in Fig. 4 show clear differences with respect to some critical distances: the degree of elongation of the carbonyl group is largest on the ATPH catalyst (1.39 Å) while it is only slightly elongated for the reaction in the gas phase. In accordance therewith, the length of the forming C—C bond is the shortest on ATPH. Thus, for ATPH, the transition state is more product-like while being more reactant-like for the reaction in gas phase. These geometrical observations are very useful in providing preliminary insight into the differences in activity of the various catalysts. On ATPH, the carbonyl bond is activated most strongly, yielding the highest positive charge on the carbon of the carbonyl group and favoring therefore the nucleophilic attack of the C=C bond. We expect therefore strongest adsorption of citronellal and highest activity toward formation of (−)-isopulegol on ATPH, followed by $ZnBr_2$ and Cu-BTC. In the next section, the activity of the various catalysts is discussed on basis of free-energy differences, which will support these findings.

It is of utmost importance to explore the free-energy surface in the region of the transition states properly to ensure that all important transition states for the determination of the selectivity calculations are taken into account (vide supra). A first explorative transition state search was performed on the $Cu_2(COO)_4$ paddlewheel (Cu-PDWL), which is a metal dimer, forming a

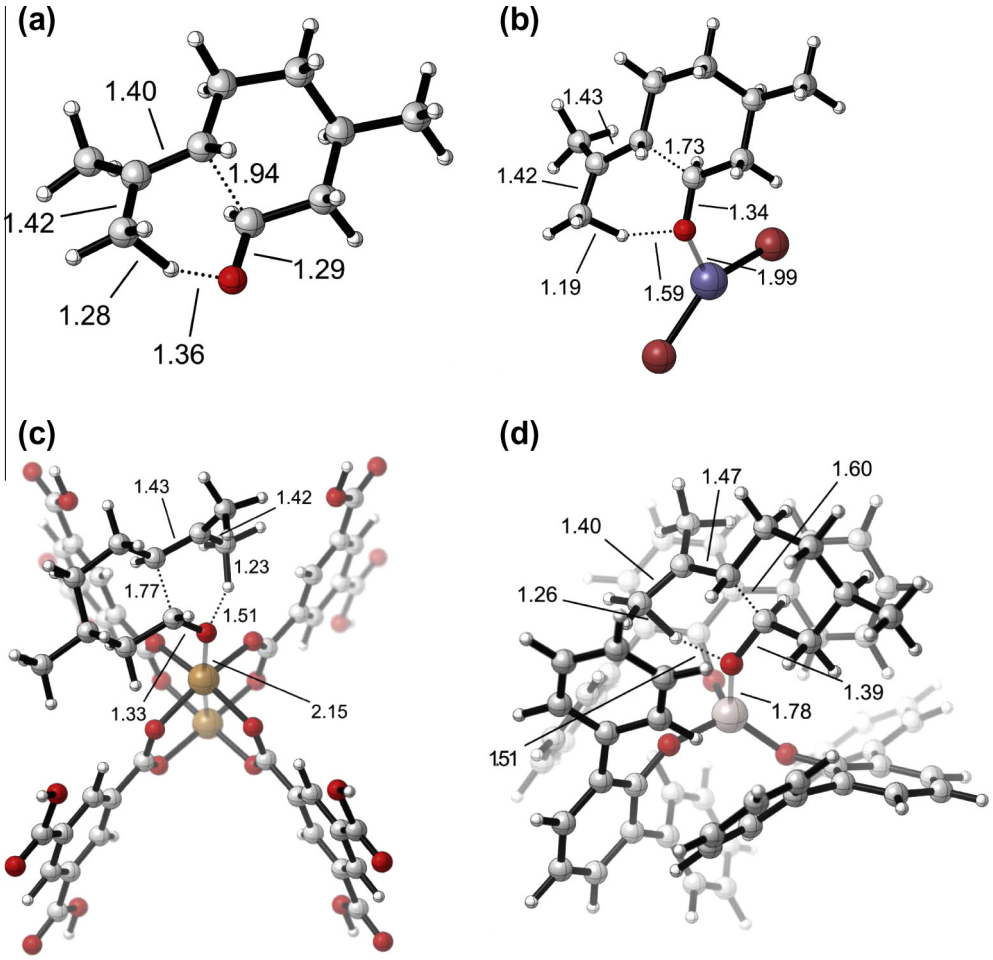

Fig. 4. Transition states for cyclization of (+)-citronellal toward (−)-isopulegol (a) in the gas phase, (b) on $ZnBr_2$, (c) on Cu-BTC, and (d) on ATPH. All transition states were localized at the B3LYP/6-31+g(d) level. Some critical distances in Å are explicitly shown.

four-coordinate square planar vertex [36,58,75,76]. The Cu-PDWL is seemingly easier to treat due to the smaller number of atoms in the metal–dimer but has proven to be quite ambitious from theoretical point of view to perform a proper transition state search. This is due to the electronic structure of open-shell transition metal cations (Cu^{2+}) and the presence of unpaired electrons on two adjacent Cu^{2+} cations, which justifies the usage of multi-reference wavefunction-based methods. Such an approach is especially needed for the study of adsorption processes as was nicely shown in the recent paper of Nachtigall et al. to study the CO adsorption in Cu-BTC [76]. But for the exploration of the potential energy surface in the neighborhood of the transition state, computationally more feasible DFT methods are largely sufficient. Selectivity predictions will be performed on the whole Cu-BTC material.

As the carbonyl oxygen has two free electron pairs, two possible adsorption geometries are possible on the Cu-PDWL, which are labeled with "1" and "2" in Fig. 5. Furthermore, the isopropyl group may be rotated which gives another two transition states labeled with "rotated isopropyl". Additionally, the forming cyclohexane ring can have various conformations, such as twisted-boat, boat, or half-chair. To investigate the occurrence of transition states with another conformation for the cyclohexane ring, we located the twisted-boat form as this one is a stable minimum on the potential energy surface (of a cyclohexane ring) in the gas phase. Following this procedure, six transition states were located. For the cyclization toward the other isomers of pulegol, a similar investigation was performed and all activated complexes are shown in Fig. S1 of the Supplementary Material (SM). From the relative free-energy differences between the various transition states (these are also indicated in Fig. 5), it is immediately clear that rotated isopropyl and twisted-boat conformers are much higher in free energy (up to 30–60 kJ/mol), and that only chair-like transition states need to be considered in the further activity and selectivity study. On the other hand, it is necessary to take into account two possible adsorption positions for the carbonyl oxygen, as there is only a difference of 3.3 kJ/mol between the iso-1-chair and iso-2-chair transition state. For the study on the other Lewis acid catalysts, we will systematically consider all possible adsorption geometries, but restricted to chair conformations.

3.2. Theoretical and experimental investigation of the catalyst activity

Experimentally, the activity of the catalysts was investigated by measuring and comparing the reaction rates on the various catalysts. The reaction rates were measured at two different temperatures: at 298 K for ATPH and $ZnBr_2$ and 373 K for Cu-BTC. At 373 K, deactivation takes place for $ZnBr_2$. Table 1 reports the experimental conditions and measured reaction rates corresponding with initial kinetic observations, i.e., at low conversion of citronellal. For each catalyst, the number of citronellal molecules converted per mol metal sites per h is given. As the cyclization reaction is first order in citronellal, the concentration of citronellal at any time is given by

$$[A] = [A]_0 . \exp(-k_x t) \quad (6)$$

with the initial concentration $[A]_0$ at $t = 0$. First-order rate constants k_x can then easily be extracted (see Figs. S4–S6 in SM).

A relative order of activity can be established from comparing the relative rates k_x obtained for the catalysts at the same temperature. ATPH is the most active catalyst, catalyzing the reaction roughly four times faster than when using the same molar amount of $ZnBr_2$ (Table 1). Although the experiment has not been done at the same temperature, Cu-BTC turns out to be the slowest catalyst. As Cu-BTC is a heterogeneous catalyst, one could expect that adsorption and desorption effects also play a role.

Table 1 reports the results of two experiments with Cu-BTC under the same initial conditions. In the first case, the catalyst

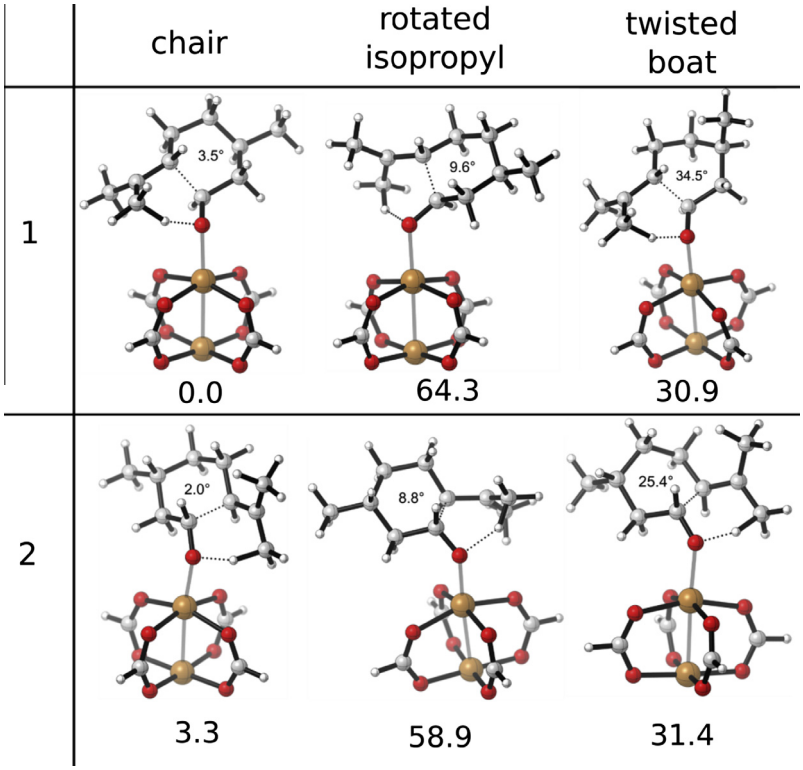

Fig. 5. Transition state geometries for cyclization of (+)-citronellal toward (−)-isopulegol on a Cu-PDWL. All transition states and energy values were localized and calculated on the B3LYP/6-31+g(d) level of theory (LANL2DZ pseudopotential and basis for Cu). Also indicated are the relative free-energy differences (in kJ/mol, at 383 K) between the various transition states, referred to the most stable transition state "iso-1-chair". Dihedral angle formed by the carbon atoms of the forming C–C bond with the two opposite carbons is given in degrees.

Table 1
Experimental pseudo-first-order rate constants and turnover frequencies for the different catalysts at given temperature.

Catalyst	g catalyst	mmol metal	mmol citronellal	T (K)	k_x (h^{-1})	Turnover frequency mmol/(h mmol)	Conversion after 8 h (%)
Cu-BTC	0.1	0.496	6.5	373	0.0087[a]	0.115[a]	7[a]
Cu-BTC	0.1	0.496	6.5	373	0.025[b]	0.295[b]	18[b]
$ZnBr_2$	0.037	0.164	16.2	298	0.19	18.7	
ATPH	0.126	0.164	16.2	298	0.83	79	

[a] Crystal particles of ~20 μm.
[b] Crystal particles of ~1–5 μm.

particles have ~10–20 μm dimensions, while in the second, the catalyst particles are much smaller (~1–5 μm) (see SEM picture in Fig. S7). The influence of the crystal size is prominent: instead of a citronellal conversion of 7% after 8 h of reaction at 373 K, the conversion increases to 18% if the size of the catalyst particles is reduced by more than half. It is a strong indication that at least in the first experiment, not all metal sites are active due to diffusion limitations of the citronellal molecules through the pores of Cu-BTC. In addition, some metal sites could be sterically blocked if an adjacent metal site is occupied by an adsorbed citronellal molecule. Consequently, such metal sites are temporarily in an inactive state. In a realistic model, we can assume that the Cu-sites located within a range of 8 Å from the active Cu-center (see Fig. S8) and situated on the surface of the same large cage are temporarily not active. Their number is estimated to be about three or four. On the other hand, the second Cu-atom on the active paddlewheel is still capable to exert its catalytic activity, at least there is no hinder for a citronellal molecule to reach it. Summarizing, apart from diffusion limitations characteristic of too large catalyst particles, only one out of four Cu-sites can simultaneously be active. This illustrates that an unambiguous correspondence between theory predictions and experimental results is not easily achieved for a heterogeneous catalyst, unless very small and uniform catalyst particles are prepared. This was previously achieved for the Zr-terephthalate MOFs of the UiO-66 type [44], but is less easy for Cu-BTC. While in Cu-BTC not all Cu-sites may participate in the citronellal cyclization, each metal in the homogeneous catalyst ZnBr2 and ATPH can be regarded as an active site.

Next, in order to complement the experiment with advanced theoretical calculations, the free-energy profiles of the citronellal cyclization toward (−)-isopulegol were constructed for all catalysts, including the adsorption and desorption steps (Fig. 6 , 373 K). The theoretical results are given in Table 2, in which also the enthalpy and entropy contributions are listed separately. The same data are also given for 298 K in the SM (Table S12). The free-energy profile is constructed based on the most stable transition state, i.e., the iso-1-chair conformation. The gas-phase results are included for the sake of completeness. In addition to the experimentally tested catalysts, we have additionally taken up a hypothetical, substituted Cu-BTC material in our theoretical test set. It concerns a Cu-BTC material which is functionalized with three electron withdrawing nitro groups on the BTC linkers, as explained in Section 2.1.2. This hypothetical material will further be referred to as Cu-BTC-NO_2 catalyst.

As expected, the uncatalyzed reaction has a high free-energy barrier of 136 kJ/mol (373 K), which consists of an enthalpy contribution of 106 kJ/mol and entropy contribution of 30 kJ/mol. During a cyclization, the entropy typically decreases. When the reaction takes place on a catalyst, the first step is an adsorption. The adsorption mode of the linear citronellal molecule on the metal is significantly different for the various catalysts (cf. Table 2). The strongest adsorption is found on ATPH (−45 kJ/mol), followed by $ZnBr_2$ (−17 kJ/mol) and for Cu-BTC there is practically no free energy of adsorption (−0.3 kJ/mol). The free energies of adsorption may be decomposed in an enthalpic and entropic contribution. A stronger

Table 2
Kinetic data for the citronellal cyclization to (−)-isopulegol at 373 K. Free-energy, enthalpic, and entropic contributions in the adsorbed state (ads) are given for linearly adsorbed citronellal (ads,citro) and adsorbed isopulegol (ads,iso) and for the transition state (‡) (kJ/mol). The rate constants (k_{373}^{fwd}) are given in units of $m^3\ mol^{-1}\ s^{-1}$ for the apparent kinetics and in s^{-1} for the intrinsic kinetics.

	$\Delta G_{373}^{ads,citro}$	$\Delta H_{373}^{ads,citro}$	$-T\cdot\Delta S_{373}^{ads,citro}$
Citronellal adsorption			
Cu-BTC	−0.28	−79.57	79.29
$ZnBr_2$	−17.36	−58.39	41.03
Cu-BTC-NO_2	−30.50	−115.81	85.31
ATPH	−44.93	−113.40	68.47
	$\Delta G_{373}^{des,iso}$	$\Delta H_{373}^{des,iso}$	$-T\cdot\Delta S_{373}^{des,iso}$
Product desorption			
Cu-BTC	32.31	99.34	−67.03
$ZnBr_2$	37.72	83.30	−45.58
Cu-BTC-NO_2	64.02	137.85	−73.83
ATPH	59.33	165.50	−70.90

	$\Delta G_{373}^{\ddagger,intr}$	$\Delta H_{373}^{\ddagger,intr}$	$T\cdot\Delta S_{373}^{\ddagger,intr}$	$k_{373}^{fwd,intr}$
Intrinsic kinetics				
Cu-BTC	92.66	77.55	15.11	8.22E−01
$ZnBr_2$	83.97	45.30	38.67	1.36E+01
Cu-BTC-NO_2	79.39	60.90	18.49	5.92E+01
ATPH	71.91	33.30	38.61	6.62E+02
	$\Delta G_{373}^{\ddagger,app}$	$\Delta H_{373}^{\ddagger,app}$	$-T\cdot\Delta S_{373}^{\ddagger,app}$	$k_{373}^{fwd,app}$
Apparent kinetics				
Gas phase	136.06	105.66	30.40	6.88E−07
Cu-BTC	92.38	−2.02	94.40	2.75E−02
$ZnBr_2$	66.61	−13.10	79.71	1.12E+02
Cu-BTC-NO_2	48.89	−54.91	103.80	3.38E+04
ATPH	26.98	−80.10	107.08	3.96E+07

Lewis acidity of the metal center gives a more negative value for the enthalpy of adsorption. The entropy contribution ($-T\Delta S$) is positive as the molecule looses three translational and three rotational degrees of freedom during adsorption and higher values are expected for catalysts which impose more steric constraints on the adsorbate. Logically, for $ZnBr_2$, the lowest value of $-T\Delta S$ is found as this catalyst imposes nearly no steric constraints on the citronellal molecule. The largest adsorption enthalpy is found for the hypothetical Cu-BTC-NO_2 material – even larger than for ATPH – and this is mainly due to the stronger Lewis acidity caused by the presence of the electron withdrawing nitro groups. The entropic contribution slightly cancels this tendency, so that in the free-energy profile, the adsorption remains the strongest on ATPH. This picture is maintained at other temperatures (Table S12).

After adsorption, the cyclization can take place, during which the citronellal molecule first assumes a non-linear conformation that is properly aligned to allow ring closure. The intrinsic kinetic data are also taken up in Table 2. These data refer to the adsorbed state of citronellal. The intrinsic free-energy barriers at 373 K vary in a limited range from 72 to 93 kJ/mol with the lowest value for ATPH and the highest value for Cu-BTC (see also Fig. 6). Depending on the specific catalytic system, this intrinsic free-energy barrier is

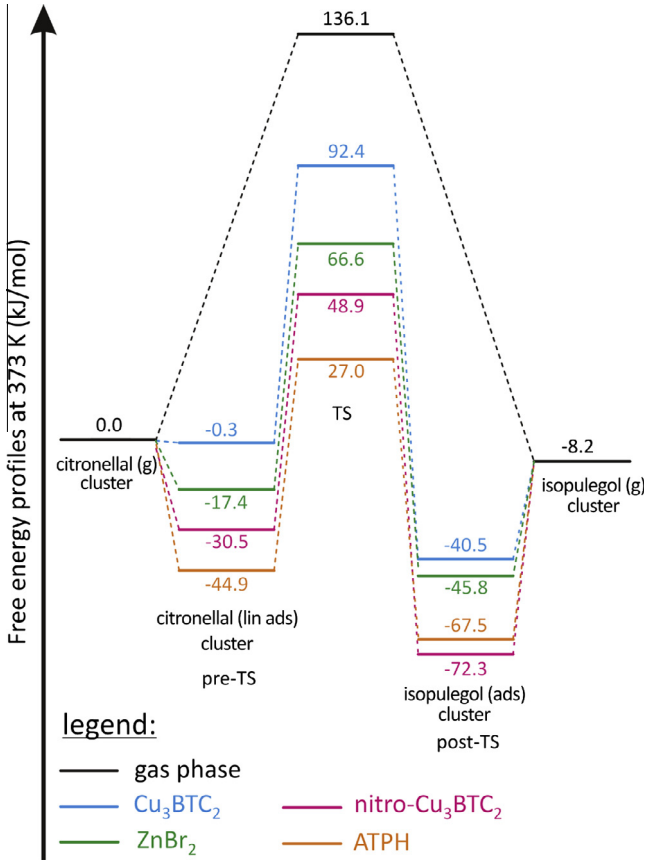

Fig. 6. Gibbs free-energy profiles, calculated at 373 K, for citronellal cyclization to (−)-isopulegol on various catalysts. The profile is based on the most stable transition state for each catalyst, the "iso-1-chair" conformation.

composed of a larger relative enthalpic or entropic contribution. The homogeneous catalysts, i.e., ATPH and $ZnBr_2$ have a larger intrinsic entropic barrier of about 39 kJ/mol. If we now assess the performance of the hypothetical Cu-BTC-NO_2 catalyst, the intrinsic free-energy barrier is about 13 kJ/mol lower than for the unsubstituted Cu-BTC. This immediately results in a predicted rate enhancement with of a factor 72, which even increases to 280 at T = 298 K. The observed increase in $k^{(intr)}$ can be ascribed to stabilization of the transition state by preferred electrostatic interactions between the adsorbate and the nitro groups, as was the case for the UiO-66-NO_2 material [44]. The transition state with indication of key geometrical parameters is shown in Fig. S17 of the Supplementary Material (SM).

In this class of reactions (cyclization of citronellal over Lewis acid metal centers), intrinsic kinetics represent a more realistic approach to simulate the experimental conversion reactions of citronellal. The same procedure has been applied for the citronellal cyclization reactions over the UiO-66 and the UiO-66-NO_2 catalysts [44]. Apparent kinetic data give rise to an overestimation.

The experiments conducted here confirmed first order kinetics in citronellal concentration. They report first-order rate constants k_x (Eq. (6), Table 1) for which at least an upper limit can easily be extracted theoretically from the intrinsic rate constants. With the experimental conditions given in Table 1 for the homogeneous catalysts, one readily derives that 0.164 mmol citronellal has been converted to isopulegol after a time period given by $1/k^{(intr)}$, leading to a conversion of 0.164/16.2 = 0.01. In the case of $ZnBr_2$ as catalyst, a theoretical k_x value of 9.44 h^{-1} is found compared with 0.19 h^{-1} experimentally (at 298 K). We notice a theoretical overestimation of a factor 50. ATPH theory predicts a k_x value of 1224 h^{-1} compared with 0.8293 h^{-1} experimentally; this implies a serious overestimation of 1476, which is not really surprising. The theoretical k_x value is derived assuming that all available adsorbed citronellal–metal complexes are converted to isopulegol at the same time and immediately followed by a next cyclization process. As long as the adsorbed isopulegol is not replaced by citronellal, a new cyclization process may not take place. Such aspects are not taken into account in the theoretical model. Within this respect, a relative comparison between k_x values of the various catalysts is more reliable. Ratios of k_x or $k^{(intr)}$ (they turn out to be the same) are shown in Table 3.

Table 3
Comparison of experimental and theoretical ratios of rate constants for the various catalysts. Theoretical results are on the B3LYP/6-311+g(d,p)-D3 level of theory and are based on the intrinsic rate coefficients. For the theory, intrinsic rate constants have been used.

	Exp	Theory	
	298 K	298 K	373 K
k_{ATPH}/k_{ZnBr2}	4.3	129	49
$k_{ZnBr2}/k_{Cu\text{-}BTC}$		225	16.5
$k_{Cu\text{-}BTC\text{-}NO2}/k_{Cu\text{-}BTC}$		280	72

Relating the theoretical intrinsic rate constant $k^{(intr)}$ for Cu-BTC with the measured catalytic activity is even more problematic as only a fraction of the metal sites is catalytically active as discussed before. Even with a realistic estimate for the effectiveness Y of the catalyst, the theoretical prediction of the conversion of citronellelal per unit time and per mol catalyst overestimates considerably the experimental value with a factor 25,000 × Y, once again demonstrating the inadequacy of the theory to predict absolute values for the observed overall catalytic performance starting from the rate constant of a single reaction.

In Table 3, the relative reaction rates are given for Cu-BTC and the hypothetical Cu-BTC-NO_2 catalyst with respect to the other Lewis acid catalysts for two temperatures 298 K and 373 K. Unfortunately, experimental information is missing as only data are available for Cu-BTC at 373 K. Nevertheless, we may say that the correct qualitative trends are found for the activities of the studied catalysts: Cu-BTC is the least active whereas ATPH gives the highest rates for the citronellal cyclization. For ATPH versus $ZnBr_2$ theory predicts a rate coefficient in favor of ATPH which is overestimated with a factor of about 129. This is probably due to the various assumptions made in the theoretical model for the description of the transition states due to the extensive number of degrees of freedom arising from the flexibility of the three (2,6-diphenyl)phenoxide ligands (see further). The hypothetical Cu-BTC-NO_2 catalyst performs much better than Cu-BTC, but less than ATPH.

3.3. Theoretical and experimental investigation of the catalyst selectivity

A good catalyst for the citronellal cyclization needs to have both a high activity and a high selectivity toward the major isomer ((−)-isopulegol). As the various studied catalysts are active within different temperature windows, it is important to assess the selectivity as a function of temperature. Experimentally, the initial selectivities at low conversion (<15%) for the citronellal cyclization were determined for ATPH, $ZnBr_2$, and Cu-BTC. Further experimental details are given in the Supplementary Material and Methods section. The experimental results for the selectivity are given in Table 4 at 373 K. It is immediately clear that the highest selectivities are obtained with ATPH (94.1% toward the (−) isopulegol isomer), followed by $ZnBr_2$ (87.5%) and finally Cu-BTC (67–73%). For this heterogeneous catalyst, the dependence of the selectivities on tem-

Table 4
Overview of the theoretical and experimental stereoselectivity distributions ((−)-isopulegol/(+)-neoisopulegol/(+)-isoisopulegol/(+)-neoisoisopulegol) on various catalysts at different temperatures. For Cu-BTC, the experimental selectivities at 373 K have been measured in two independent experiments.

T	Theory			Experiment	
	273	298	373		
Without catalyst					
iso	88.9	86.7	80.1		
neoiso	9.4	11.0	15.3		
isoiso	1.5	2.1	3.9		
neoisoiso	0.1	0.2	0.7		
Cu-BTC extended cluster				373[a]	373[b]
iso	91.1	89.1	83.3	73	67.0
neoiso	7.3	8.7	12.3	20.8	21.7
isoiso	1.5	2.1	4.1	6.2	11.2
neoisoiso	0	0.1	0.2	<0.2	<0.2
Cu-BTC periodic					
iso	92.5	91	85.9	73	67.0
neoiso	1.2	1.9	4.4	20.8	21.7
isoiso	6.3	7.1	9.6	6.2	11.2
neoisoiso	0	0	0.1		
ATPH				298	
iso	91.6	90.6	88.1	94.1	
neoiso	0.0	0.1	0.2	1.0	
isoiso	8.4	9.3	11.8	4.3	
neoisoiso	0.0	0.0	0.0	0.6	
$ZnBr_2$				298	
iso	91.6	89.4	82.5	87.5	
neoiso	5.8	7.2	11.0	7.4	
isoiso	2.4	3.2	5.9	5.1	
neoisoiso	0.1	0.2	0.6	<0.1	

[a] With crystal particles of size 20 μm.
[b] With crystal particles of size 1–5 μm.

Table 5
Experimental selectivities at different temperatures toward the isopulegol isomers in the citronellal cyclization with Cu-BTC as a catalyst.

T (K)	S_{iso}	S_{neoiso}	$S_{(isoiso+neoisoiso)}$
373	73.0	20.8	6.2
423	67.5	24.8	7.7
443	66.9	24.5	8.6
463	66.2	24.8	9
483	65.6	24.8	9.6

perature shows that the selectivity toward the major isopulegol isomer drops when increasing the temperature (Table 5).

To rationalize these diastereoselectivities, selectivities were calculated using the Curtin-Hammett principle giving initial selectivities $S_{i,ini}$. The computational results on the initial selectivities are critically dependent on the construction of a representative set of stereoisomeric transition states.

For all catalysts, the most relevant diastereomeric transition states, determining the theoretical selectivities, are given in the Supplementary Material. In the search for these structures, all possible adsorption sites for the carbonyl bond have been taken into account.

Fig. 7 shows the selectivity for the desired (−)-isopulegol diastereomer **2**, obtained using the selectivity expression (Eqs. (2) and (3)) and for the different catalysts in terms of temperature.

Theoretical values for the diastereoselectivity distributions are also taken up in Table 4 together with the experimental values to allow a straightforward comparison. Additionally, the relative free-energy differences between the stereoselective transition states are given in Table 6. The most significant result is found for ATPH, predicting an initial theoretical selectivity at 298 K of 90.6%. Apart from being the most active catalyst, it also improves the diastereoselectivity toward the desired product as the differences in free energy of activation between the (−)-isopulegol and the other stereoisomers are most pronounced (6.25 kJ/mol (isoiso), 19.39 kJ/mol (neoiso), 37.51 kJ/mol (neoisoiso)). Experimental selectivities are measured at 298 K. The agreement with the theoretical predictions is fairly good (Table 4). It is highly remarkable that both theory and experiment predict the isoiso diastereomer as second most abundant product. For the other Lewis acid catalysts, $ZnBr_2$ and Cu-BTC, the second most abundant stereomer is neoiso, with free-energy differences of about 5 kJ/mol justifying the initial selectivities as indicated in Table 4. For the heterogeneous catalyst, Cu-BTC also periodic calculations have been performed taking into account the full molecular environment around the Lewis acid site. The selectivities using the periodic model are also shown in Table 4. The periodic calculations do not predict large deviations of the observed selectivities toward (−)-isopulegol with respect to the extended cluster model but switches the type of second most abundant stereomer.

Interestingly, the diastereoselectivity seems to decrease less fast in terms of temperature for ATPH than for the other catalysts (see Fig. 7). This originates from the difference in free energies between the stereoselective transition states, which increases in terms of temperature for ATPH (the values are taken up in Table S11 of the SM). This effect is mainly due to the variations in the entropic barrier. For ATPH, the apparent entropic barrier is the largest (107 kJ/mol as taken up in Table 4), due to the strong steric hindrance of the bulky ligands around the catalytic center. For the sake of completeness, additional selectivity profiles for all catalysts have been taken up in the SM (Figs. S9–S13).

A comparison between the theoretical and experimental diastereoselectivities learns that the overall agreement is fairly well, taking into account the small energy differences predicted between the various stereomers ranging between 5 and 10 kJ/mol. The prediction of such data is very sensitive to the used model, such as the level of theory. We calculated the selectivities using various functionals (TPSS, M06-2X, M06-L, and B3LYP) and found that the B3LYP functional yielded the closest approximation with experimental results for $ZnBr_2$ and Cu-BTC, and we have therefore retained these results. The differences in free energies between the set of stereoselective transition states at other levels of theory are taken up in Tables S14 and S15 of the SM.

For both ATPH and $ZnBr_2$, the agreement with $S_{i,ini}$ is more than satisfactory and the agreement proves that the observed selectivities are kinetically controlled by the forward reactions. For these catalysts, there is no diffusion limitation which could mask the initial selectivities in the measured data (cf. Table 4 and Fig. 7).

For Cu-BTC, the experimental values do not coincide with the initial selectivities but are much lower. The activity experiments already pointed out that Cu-BTC is a typical example where diffusion limitations might play an important role. The pore size limitation is also illustrated in Fig. 1.

For the sake of completeness, also the thermodynamically determined selectivities are plotted in Fig. 7b for various levels of theory. The results reveal that all catalysts enhance the selectivity toward isopulegol as expected. Some caution is however needed since these selectivity profiles are also quite sensitive to the used theoretical method.

Finally, it is interesting to comment on the theoretical predictions for the selectivities of a hypothetical nitro substituted version of the Cu-BTC material. The initial selectivities toward (−)-isopulegol are very high with values larger than 95%. This catalyst has similarities with the highly selective homogeneous ATPH catalyst. The additional nitro groups enhance the Lewis acidity of the metal centers, thus making this material more active than the unsubstituted Cu-BTC material and additionally the nitro groups impose

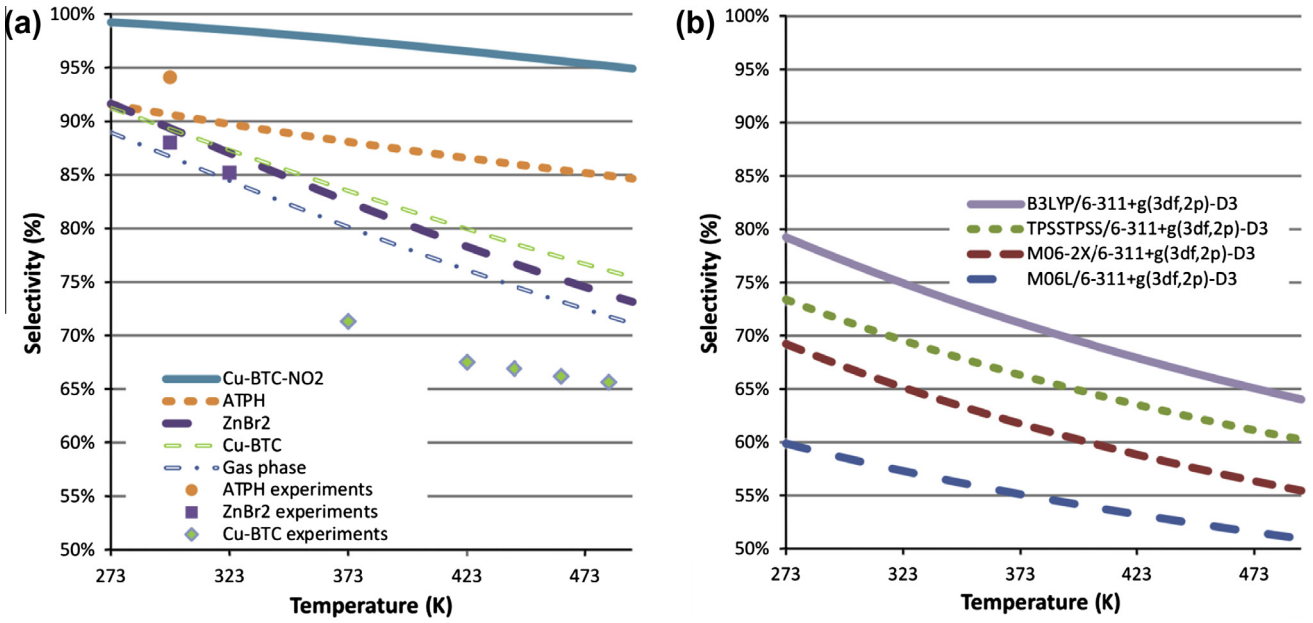

Fig. 7. (a) Theoretical diastereoselectivity toward (−)-isopulegol on various catalysts (ATPH, $ZnBr_2$, Cu-BTC, Cu-BTC-NO_2, and for a non-catalyzed gas-phase reaction; (b) thermodynamic product selectivity in function of the used level of theory.

Table 6
Relative free-energy differences ($\Delta(\Delta G^{\ddagger}_{373})$, kJ/mol) at 373 K between the different transition states toward the various pulegol isomers.

	Gas phase	$ZnBr_2$	ATPH	Cu-BTC
iso	0.00	0.00 1.16	0.00	0.00 2.65 7.08 7.95
neoiso	5.14	4.62	19.39	5.55 10.40 12.39 12.66
isoiso	9.34	8.61 8.85	6.25	10.93 11.07 12.57 16.82
neoisoiso	14.79	13.53	37.51	17.77 20.66

additional steric hindrance which favors formation of the desired (−)-isopulegol. Also for this Cu-BTC-NO_2 catalyst, a high entropy barrier is found as in ATPH (Table S6 of SM). However, the Cu-BTC framework is not ideally suited for high selectivities toward isopulegol in reality due to pore restrictions, which inhibit fast diffusion of the various products. A realistic catalyst for practical purposes would need larger pores. Modifying the dimensions of the linkers without truly altering the active site is actively explored within the MOF community [77–80,81].

4. Conclusions

In this paper, we evaluated the performance of various Lewis acid catalysts for the enantioselective cyclization of (+)-citronellal toward (−)-isopulegol. We have performed a combined experimental and theoretical study to unravel the catalytic mechanisms and characteristics in order to rationalize both the activity of the catalyst and selectivity toward the desired stereomer. Our test set contains the Lewis acid catalysts $ZnBr_2$, ATPH, and Cu-BTC. ATPH is the most active catalyst, characterized by the highest reaction rates toward (−)-isopulegol, and the heterogeneous metal organic framework Cu-BTC turns out to be the least active. The activity is directly related to the strength of the Lewis acid metal centers. A stronger acidity activates the carbonyl bond more strongly, leading to a transition state which is more product-like and a larger positive charge on the carbonyl carbon which favors nucleophilic attack of the carbon–carbon double bond. Experiments on Cu-BTC also reveal that the catalytical conversion is strongly dependent on the size of the catalyst particles due to diffusional restrictions (e.g., due to blocked channels and pores). Small particles of size 1–5 μm are used in order to get the highest efficiency.

The theoretical selectivity is controlled by the free-energy differences between the diastereomeric transition states. ATPH is very selective toward (−)-isopulegol with an experimentally determined selectivity at 298 K of about 94% and – following theory – a less decrease in selectivity with temperature. $ZnBr_2$ has a selectivity of 87.5% at 298 K, whereas Cu-BTC turns out to be the least selective. The high selectivity of ATPH may be traced back to a favorable free-energy entropic barrier toward the major diastereomer compared with the other isomers. For $ZnBr_2$ and Cu-BTC, the selectivities toward (−)-isopulegol decrease significantly for higher temperatures. Thus, ATPH fulfils the requirements for the most ideal catalyst: it shows a high activity at low temperatures and is most selective toward the major isomer. Based on these insights, we simulated the selectivities of a hypothetical Cu-BTC material which was additionally functionalized with nitro groups. As such more steric hindrance was introduced which indeed predicts a higher selectivity toward (−)-isopulegol.

Overall, the agreement between the theoretically predicted selectivities and experimentally measured values is very good. The theoretical prediction of enantioselectivities is highly ambitious within computational chemistry as it depends on a representative set of stereoselective transition states and the ability of theoretical methods to calculate accurately the free-energy differences between the various activated complexes. The combined experimental and theoretical approach followed here is a case study for rational design of asymmetric catalysts as it reveals the

major factors contributing to selectivity and activity of the Lewis acid catalyst.

Acknowledgments

This work is supported by the Research Board of Ghent University (BOF), the Fund for Scientific Research; Flanders (FWO), and BELSPO in the frame of IAP/6/27. Funding was also received from the European Research Council under the European Community's Seventh Framework Programme [FP7(2007-2013) ERC Grant Agreement No. 240483]. We would also like to thank Petr Nachtigall and Lukáš Grajciar for providing us with the optimized Cu-BTC unit cell. The computational resources (Stevin Supercomputer Infrastructure) and services used in this work were provided by Ghent University.

Appendix A. Supplementary material

Supplementary data associated with this article can be found, in the online version, at http://dx.doi.org/10.1016/j.jcat.2013.04.017.

References

[1] J.C. Leffingwell, D. Leffingwel, Chiral Chemistry in Flavours & Fragrances, Speciality Chemicals Magazine, 2011, pp. 30–33.
[2] B. Lawrence, R. Hopp, Natural and Synthetic Menthol, CRC Press, 2006.
[3] T. Iwata, Y. Okeda, Y. Hori, Process for Producing Isopulegol, Takasago International Corporation, United States, 2002. p. 9.
[4] C. Milone, C. Gangemi, G. Neri, A. Pistone, S. Galvagno, Selective one step synthesis of (−)menthol from (+)citronellal on Ru supported on modified SiO(2), Appl. Catal. A – Gen. 199 (2000) 239–244.
[5] C. Milone, A. Perri, A. Pistone, G. Neri, S. Galvagno, Isomerisation of (+)citronellal over Zn(II) supported catalysts, Appl. Catal. A – Gen. 233 (2002) 151–157.
[6] P.J. Kropp, G.W. Breton, S.L. Craig, S.D. Crawford, W.F. Durland, J.E. Jones, J.S. Raleigh, Surface-mediated reactions. 6. Effects of silica-gel and alumina on acid-catalyzed reactions, J. Org. Chem. 60 (1995) 4146–4152.
[7] M. Friedrich, K. Ebel, N. Götz, Method for the Production of Isopulegol, BASF SE, Ludwigshafen (DE), 2009, p. 9.
[8] M. Friedrich, K. Ebel, N. Gotz, W. Krausee, C. Zahm, Diarylphenoxy Aluminium Compounds, BASF SE, US 7,608,742 B2, 2009.
[9] G. Heydrich, G. Gralla, K. Ebel, M. Friedrich, Recovery of phenol Ligands During the Production of Isopulegol, BASF SE, US 8,003,829 B2, 2011.
[10] G. Heydrich, G. Gralla, M. Rauls, J. Schmidt-Leithoff, K. Ebel, W. Krause, S. Oehlenschlager, C. Jakel, M. Friedrich, J. Bergner, N. Kashani-Shirazi, R. Paciello, Method for Producing Optically Active, Racemic Menthol, BASF SE, US 2010/0249467 A1, 2010.
[11] H. Itoh, Y. Hori, Aluminum Complex and Use thereof, 2011.
[12] M. Boronat, P. Concepcion, A. Corma, M.T. Navarro, M. Renz, S. Valencia, Reactivity in the confined spaces of zeolites: the interplay between spectroscopy and theory to develop structure–activity relationships for catalysis, Phys. Chem. Chem. Phys. 11 (2009) 2876–2884.
[13] M. Boronat, A. Corma, M. Renz, Turning Points in Solid-State, Materials and Surface Science, The Royal Society of Chemistry, 2008.
[14] A. Corma, M. Renz, Sn-Beta zeolite as diastereoselective water-resistant heterogeneous Lewis-acid catalyst for carbon–carbon bond formation in the intramolecular carbonyl-ene reaction, Chem. Commun. (2004) 550–551.
[15] Z. Yongzhong, N. Yuntong, S. Jaenicke, G.-K. Chuah, Cyclisation of citronellal over zirconium zeolite beta—a highly diastereoselective catalyst to (±)-isopulegol, J. Catal. 229 (2005) 404–413.
[16] A.U. Czaja, N. Trukhan, U. Muller, Industrial applications of metal–organic frameworks, Chem. Soc. Rev. 38 (2009).
[17] G. Férey, C. Serre, T. Devic, G. Maurin, H. Jobic, P.L. Llewellyn, G. De Weireld, A. Vimont, M. Daturi, J.-S. Chang, Why hybrid porous solids capture greenhouse gases?, Chem Soc. Rev. 40 (2011) 550–562.
[18] S.S. Han, J.L. Mendoza-Cortes, W.A. Goddard Iii, Recent advances on simulation and theory of hydrogen storage in metal–organic frameworks and covalent organic frameworks, Chem. Soc. Rev. 38 (2009) 1460–1476.
[19] L.J. Murray, M. Dinca, J.R. Long, Hydrogen storage in metal–organic frameworks, Chem. Soc. Rev. 38 (2009) 1294–1314.
[20] J.L.C. Rowsell, A.R. Millward, K.S. Park, O.M. Yaghi, Hydrogen sorption in functionalized metal–organic frameworks, J. Am. Chem. Soc. 126 (2004) 5666–5667.
[21] M.P. Suh, H.J. Park, T.K. Prasad, D.-W. Lim, Hydrogen storage in metal–organic frameworks, Chem. Rev. 112 (2012) 782–835.
[22] R.J. Kuppler, D.J. Timmons, Q.R. Fang, J.R. Li, T.A. Makal, M.D. Young, D.Q. Yuan, D. Zhao, W.J. Zhuang, H.C. Zhou, Potential applications of metal–organic frameworks, Coord. Chem. Rev. 253 (2009) 3042–3066.
[23] J.R. Li, R.J. Kuppler, H.C. Zhou, Selective gas adsorption and separation in metal–organic frameworks, Chem. Soc. Rev. 38 (2009) 1477–1504.
[24] J. Gascon, F. Kapteijn, Metal-Organic Framework Membranes-High Potential, Bright Future? Angew, Chem.-Int. Ed. 49 (2010) 1530–1532.
[25] J.-R. Li, J. Sculley, H.-C. Zhou, Metal–organic frameworks for separations, Chem. Rev. 112 (2012) 869–932.
[26] Y. Liu, W. Xuan, Y. Cui, Engineering homochiral metal–organic frameworks for heterogeneous asymmetric catalysis and enantioselective separation, Adv. Mater. 22 (2010) 4112–4135.
[27] M.D. Allendorf, C.A. Bauer, R.K. Bhakta, R.J.T. Houk, Luminescent metal–organic frameworks, Chem. Soc. Rev. 38 (2009) 1330–1352.
[28] L.D. Carlos, R.A.S. Ferreira, V. de Zea Bermudez, B. Julian-Lopez, P. Escribano, Progress on lanthanide-based organic–inorganic hybrid phosphors, Chem. Soc. Rev. 40 (2011) 536–549.
[29] J. Rocha, L.D. Carlos, F.A.A. Paz, D. Ananias, Luminescent multifunctional lanthanides-based metal–organic frameworks, Chem. Soc. Rev. 40 (2011) 926–940.
[30] M. Kurmoo, Magnetic metal–organic frameworks, Chem. Soc. Rev. 38 (2009) 1353–1379.
[31] J. Lee, O.K. Farha, J. Roberts, K.A. Scheidt, S.T. Nguyen, J.T. Hupp, Metal–organic framework materials as catalysts, Chem. Soc. Rev. 38 (2009) 1450–1459.
[32] D. Farrusseng, S. Aguado, C. Pinel, Metal–organic frameworks: opportunities for catalysis, Angew. Chem. – Int. Ed. 48 (2009) 7502–7513.
[33] L. Ma, C. Abney, W. Lin, Enantioselective catalysis with homochiral metal–organic frameworks, Chem. Soc. Rev. 38 (2009) 1248–1256.
[34] M. Yoon, R. Srirambalaji, K. Kim, Homochiral metal–organic frameworks for asymmetric heterogeneous catalysis, Chem. Rev. 112 (2012) 1196–1231.
[35] L. Alaerts, E. Seguin, H. Poelman, F. Thibault-Starzyk, P.A. Jacobs, D.E. De Vos, Probing the Lewis acidity and catalytic activity of the metal–organic framework Cu-3(btc)(2) (BTC = benzene-1,3,5-tricarboxylate), Chem. – Eur. J. 12 (2006) 7353–7363.
[36] S.S.Y. Chui, S.M.F. Lo, J.P.H. Charmant, A.G. Orpen, I.D. Williams, A chemically functionalizable nanoporous material Cu-3(TMA)(2)(H_2O)(3) (n), Science 283 (1999) 1148–1150.
[37] D.J. Tranchemontagne, J.R. Hunt, O.M. Yaghi, Room temperature synthesis of metal–organic frameworks: MOF-5, MOF-74, MOF-177, MOF-199, and IRMOF-0, Tetrahedron 64 (2008) 8553–8557.
[38] S. De Rosa, G. Giordano, T. Granato, A. Katovic, A. Siciliano, F. Tripicchio, Chemical pretreatment of olive oil mill wastewater using a metal–organic framework catalyst, J. Agric. Food Chem. 53 (2005) 8306–8309.
[39] E. Perez-Mayoral, J. Cejka, Cu-3(BTC)(2): a metal–organic framework catalyst for the Friedlander reaction, ChemCatChem 3 (2011) 157–159.
[40] K. Schlichte, T. Kratzke, S. Kaskel, Improved synthesis, thermal stability and catalytic properties of the metal–organic framework compound CU3(BTC)(2), Microporous Mesoporous Mater. 73 (2004) 81–88.
[41] Y. Wu, L.G. Qiu, W. Wang, Z.Q. Li, T. Xu, Z.Y. Wu, X. Jiang, Kinetics of oxidation of hydroquinone to p-benzoquinone catalyzed by microporous metal–organic frameworks M-3(BTC)(2) M = copper(II), cobalt(II), or nickel(II); BTC = benzene-1,3,5-tricarboxylate using molecular oxygen, Transition Met. Chem. 34 (2009) 263–268.
[42] S. Marx, W. Kleist, A. Baiker, Synthesis, structural properties, and catalytic behavior of Cu-BTC and mixed-linker Cu-BTC-PyDC in the oxidation of benzene derivatives, J. Catal. 281 (2011) 76–87.
[43] BASF, BASF Press Release: BASF Adds L-menthol to Product Range, June 1, 2010.
[44] F. Vermoortele, M. Vandichel, B. Van de Voorde, R. Ameloot, M. Waroquier, V. Van Speybroeck, D.E. De Vos, Electronic effects of linker substitution on lewis acid catalysis with metal–organic frameworks, Angew. Chem. – Int. Ed. 51 (2012) 4887–4890.
[45] A. Ghysels, D. Van Neck, M. Waroquier, Cartesian formulation of the mobile block Hessian approach to vibrational analysis in partially optimized systems, J. Chem. Phys. 127 (2007) 164108.
[46] P.J. Hay, W.R. Wadt, Abinitio effective core potentials for molecular calculations – potentials for the transition-metal atoms Sc to Hg, J. Chem. Phys. 82 (1985) 270–283.
[47] S. Grimme, J. Antony, S. Ehrlich, H. Krieg, A consistent and accurate ab initio parametrization of density functional dispersion correction (DFT-D) for the 94 elements H–Pu, J. Chem. Phys. 132 (2010).
[48] Y. Zhao, D.G. Truhlar, The M06 suite of density functionals for main group thermochemistry, thermochemical kinetics, noncovalent interactions, excited states, and transition elements: two new functionals and systematic testing of four M06-class functionals and 12 other functionals, Theor. Chem. Acc. 120 (2008) 215–241.
[49] Y. Zhao, D.G. Truhlar, Density functionals with broad applicability in chemistry, Acc. Chem. Res. 41 (2008) 157–167.
[50] S. Catak, K. Hemelsoet, L. Hermosilla, M. Waroquier, V. Van Speybroeck, Competitive reactions of organophosphorus radicals on coke surfaces, Chem. – Eur. J. 17 (2011) 12027–12036.
[51] S. Catak, M. D'Hooghe, N. De Kimpe, M. Waroquier, V. Van Speybroeck, Intramolecular pi-pi stacking interactions in 2-substituted N,N-dibenzylaziridinium ions and their regioselectivity in nucleophilic ring-opening reactions, J. Org. Chem. 75 (2010) 885–896.
[52] K. Leus, M. Vandichel, Y.Y. Liu, I. Muylaert, J. Musschoot, S. Pyl, H. Vrielinck, F. Callens, G.B. Marin, C. Detavernier, P.V. Wiper, Y.Z. Khimyak, M. Waroquier, V. Van Speybroeck, P. Van der Voort, The coordinatively saturated vanadium MIL-

47 as a low leaching heterogeneous catalyst in the oxidation of cyclohexene, J. Catal. 285 (2012) 196–207.
[53] T. Verstraelen, V. Van Speybroeck, M. Waroquier, ZEOBUILDER: a GUI toolkit for the construction of complex molecular structures on the nanoscale with building blocks, J. Chem. Inf. Model. 48 (2008) 1530–1541.
[54] G. Kresse, J. Hafner, Ab initio molecular-dynamics simulation of the liquid–metal-amorphous-semiconductor transition in germanium, Phys. Rev. B 49 (1994) 14251.
[55] G. Kresse, J. Hafner, Ab initio molecular dynamics for liquid metals, Phys. Rev. B 47 (1993) 558.
[56] G. Kresse, J. Furthmüller, Efficient iterative schemes for ab initio total-energy calculations using a plane-wave basis set, Phys. Rev. B 54 (1996) 11169.
[57] G. Kresse, J. Furthmüller, Efficiency of ab-initio total energy calculations for metals and semiconductors using a plane-wave basis set, Comput. Mater. Sci. 6 (1996) 15.
[58] L. Grajciar, O. Bludsky, P. Nachtigall, Water adsorption on coordinatively unsaturated sites in CuBTC MOF, J. Phys. Chem. Lett. 1 (2010) 3354–3359.
[59] J.P. Perdew, K. Burke, M. Ernzerhof, Generalized gradient approximation made simple, Phys. Rev. Lett. 77 (1996) 3865.
[60] J.P. Perdew, K. Burke, M. Ernzerhof, Erratum: generalized gradient approximation made simple, Phys. Rev. Lett. 78 (1997) 1396.
[61] P.E. Blöchl, Projector augmented-wave method, Phys. Rev. B 50 (1994) 17953.
[62] S. Grimme, Semiempirical GGA-type density functional constructed with a long-range dispersion correction, J. Comput. Chem. 27 (2006) 1787–1799.
[63] B.A. De Moor, A. Ghysels, M.F. Reyniers, V. Van Speybroeck, M. Waroquier, G.B. Marin, Normal mode analysis in zeolites: toward an efficient calculation of adsorption entropies, J. Chem. Theory Comput. 7 (2011) 1090–1101.
[64] M.T. Reetz, A. Meiswinkel, G. Mehler, K. Angermund, M. Graf, W. Thiel, R. Mynott, D.G. Blackmond, Why are BINOL-based monophosphites such efficient ligands in Rh-catalyzed asymmetric olefin hydrogenation?, J Am. Chem. Soc. 127 (2005) 10305–10313.
[65] P.J. Donoghue, P. Helquist, P.-O. Norrby, O. Wiest, Development of a Q2MM force field for the asymmetric rhodium catalyzed hydrogenation of enamides, J. Chem. Theory Comput. 4 (2008) 1313–1323.
[66] J.I.h.o.w.c.d.c.p. Seeman, Effect of conformational change on reactivity in organic chemistry. Evaluations, applications, and extensions of Curtin-Hammett Winstein-Holness kinetics, Chem. Rev. 83 (1983) 83–134.
[67] I. Takeshi, O. Yoshiki, H. Yoji, Takasago Perfumery Co. Ltd., EP1225163 (A2), 2002.
[68] Y.K. Seo, G. Hundal, I.T. Jang, Y.K. Hwang, C.H. Jun, J.S. Chang, Microwave synthesis of hybrid inorganic-organic materials including porous Cu-3(BTC)(2) from Cu(II)-trimesate mixture, Microporous Mesoporous Mater. 119 (2009) 331–337.
[69] S. Choomwattana, T. Maihom, P. Khongpracha, M. Probst, J. Limtrakul, Structures and mechanisms of the carbonyl-ene reaction between MOF-11 encapsulated formaldehyde and propylene: an ONIOM study, J. Phys. Chem. C 112 (2008) 10855–10861.
[70] S. Wannakao, P. Khongpracha, J. Limtrakul, Density functional theory study of the carbonyl-ene reaction of encapsulated formaldehyde in Cu(I), Ag(I), and Au(I) exchanged FAU zeolites, J. Phys. Chem. A 115 (2011) 12486–12492.
[71] Q.W. Yang, X.L. Tong, W.Q. Zhang, Influence of Lewis acids and substituents on carbonyl-ene reactions: a density functional theory study, J. Mol. Struct. – Theochem 957 (2010) 84–89.
[72] K. Mikami, M. Shimizu, Asymmetric ene reactions in organic-synthesis, Chem. Rev. 92 (1992) 1021–1050.
[73] Y. Kikukawa, S. Yamaguchi, Y. Nakagawa, K. Uehara, S. Uchida, K. Yamaguchi, N. Mizuno, Synthesis of a dialuminum-substituted silicotungstate and the diastereoselective cyclization of citronellal derivatives, J. Am. Chem. Soc. 130 (2008) 15872–15878.
[74] M.R. Zardoost, M.R. Gholami, M. Irani, S.A. Siadati, A density functional theory study of cyclization of citronellal, Prog. React. Kinet. Mech. 37 (2012) 173–182.
[75] D. Sun, S. Ma, Y. Ke, D.J. Collins, H.-C. Zhou, An interweaving MOF with high hydrogen uptake, J. Am. Chem. Soc. 128 (2006) 3896–3897.
[76] M. Rubes, L. Grajciar, O. Bludsky, A.D. Wiersum, P.L. Llewellyn, P. Nachtigall, Combined theoretical and experimental investigation of CO adsorption on coordinatively unsaturated sites in CuBTC MOF, ChemPhysChem 13 (2012) 488–495.
[77] B.L. Chen, M. Eddaoudi, S.T. Hyde, M. O'Keeffe, O.M. Yaghi, Interwoven metal–organic framework on a periodic minimal surface with extra-large pores, Science 291 (2001) 1021–1023.
[78] H. Furukawa, Y.B. Go, N. Ko, Y.K. Park, F.J. Uribe-Romo, J. Kim, M. O'Keeffe, O.M. Yaghi, Isoreticular expansion of metal–organic frameworks with triangular and square building units and the lowest calculated density for porous crystals, Inorg. Chem. 50 (2011) 9147–9152.
[79] S.E. Wenzel, M. Fischer, F. Hoffmann, M. Froba, Highly porous metal–organic framework containing a novel organosilicon linker – a promising material for hydrogen storage, Inorg. Chem. 48 (2009) 6559–6565.
[80] K.A. Cychosz, A.G. Wong-Foy, A.J. Matzger, Liquid phase adsorption by microporous coordination polymers: removal of organosulfur compounds, J. Am. Chem. Soc. 130 (2008) 6938–6939.
[81] A. Vimont, F. Thibault-Starzyk, M. Daturi, Analysing and understanding the active site by IR spectroscopy, Chem. Soc. Rev. 39 (2010) 4928–4950.